

The ESO Nearby Abell Cluster Survey ^{*} ^{**}

IV. The Fundamental Plane of clusters of galaxies

C. Adami¹, A. Mazure¹, A. Biviano², P. Katgert³, G. Rhee⁴

¹ IGRAP, Laboratoire d'Astronomie Spatiale, Marseille, France

² TeSRE, CNR, Bologna, Italy

³ Sterrewacht Leiden, The Netherlands

⁴ University of Nevada, Las Vegas, U.S.A.

Received date; accepted date

Abstract. We have used the ESO Nearby Abell Cluster Survey (ENACS) in combination with the Cosmos Galaxy Catalogue, to investigate the existence of a Fundamental Plane (FP) for rich clusters of galaxies. The 20 clusters with the most regular projected galaxy distributions appear to define a quite narrow FP, which is similar to the FP found by Schaeffer et al., who used other clusters. Our cluster FP appears to be different from that of ellipticals, as well as from the virial prediction. The latter fact may have several physical explanations, or a combination thereof. If M/L varies with L this will change the FP slope away from the virial slope. Differences in dynamical structure between clusters will also produce deviations from the virial FP. In view of the long virialization time-scales in all but the very central parts of galaxy clusters, the deviation of the cluster FP from the virial expectation may also result from clusters not being totally virialized. The scatter of the observations around the cluster FP is fairly small. An important part of the observed scatter is likely to be intrinsic. If this intrinsic spread were due exclusively to deviations from the Hubble flow it would imply cluster peculiar velocities of at most about 1000 km s^{-1} .

have formed. Some clues about the answer to this question may be provided by studying their intrinsic properties, such as size, internal kinetic energy, and luminosity, as well as the relations between these properties.

Elliptical galaxies are, e.g., known to populate a two dimensional manifold in the (R, σ_v, L) -space, referred to as the "fundamental plane" (FP hereafter; Djorgovski & Davis 1987, Dressler et al. 1987); this relation between R , σ_v and L has been interpreted as arising from the virial equilibrium of these systems. In virial equilibrium, there is a relation between R , σ_v , and M (instead of L). In order to understand the FP as arising from the virial relation, a non-constant mass-to-light ratio is required for the ellipticals, viz. $M/L \propto M^{0.16}$ (e.g. Pahre et al. 1995).

The deviation from a constant M/L ratio could be the result of differences in the stellar population among ellipticals (e.g. Renzini & Ciotti 1993), or of a partly dissipative formation process (Capelato et al. 1995). The tilt of the FP relative to a constant M/L is also observed in the infra-red, where metallicity effects are much reduced with respect to the optical (Pahre et al. 1995). This may suggest that such a tilt is due to deviations from homology in ellipticals as apparent in the correlations between light-profile shape and r_e or M_B (as described by, e.g. Caon et al. 1993 or Graham et al. 1996).

It has been shown through simulations that mergers of non-homologous systems can produce a FP which slightly deviates from the expectation from the virial condition (Capelato et al. 1995). The fact that dwarf ellipticals do not follow the same relation as regular ellipticals (Bender et al. 1993) may then indicate a different formation process for the two classes or, more simply, that interactions have a different impact for large and small galaxies (Levine 1996).

The FP is also important as a distance indicator, since σ_v is a distance-independent quantity, while L and R both depend on the distance with different scaling laws. Before the FP was established, the relation between σ_v and L

Key words: Cosmology: observations- Galaxies: clusters: general -Galaxies: clustering

1. Introduction

One of the fundamental questions of modern cosmology is how the gravitationally bound systems in our Universe

Send offprint requests to: C. Adami

* Based on observations collected at the European Southern Observatory (La Silla, Chile)

** <http://www.astrsp-mrs.fr/www/enacs.html>

found by Faber & Jackson (1976) was used as a secondary distance indicator for ellipticals (similar to the relation discovered by Tully & Fisher (1977) for spiral galaxies).

Schaeffer et al. (1993) (hereafter S93) concluded on the basis of a sample of 16 galaxy clusters that these systems also populate a FP. They used a compilation by West, Dekel & Oemler (1989) of photometric data, and velocity dispersions for Abell clusters from Struble & Rood (1991). Schaeffer et al. also concluded that apparently there is a similar FP for all bound systems, which they supposed to span 9 orders of magnitudes in luminosity! This result was interpreted in the context of the hierarchical structure formation scenario, as an indication that globular clusters, galaxies and galaxy clusters have similar formation processes. The dispersion in the FP should then reflect the dispersion in the formation epoch.

There are several reasons for re-examining the existence and properties of a possible FP of clusters. First, the cluster sample used by S93 is rather heterogeneous: velocity dispersions and interloper corrections have not been derived in the same way for all clusters, and photometric data come from about 20 different sources. Moreover, S93 use as characteristic scale the de Vaucouleurs radius; however, as shown in Adami et al. (1998) (hereafter paper VII) the de Vaucouleurs profile gives a poor fit to the observed density profile of galaxy clusters. Indeed, we show in paper VII that this profile is too cusped within the central 100 kpc. For these reasons, the potentially important result of S93 needs confirmation. In the present paper, we re-examine the evidence for a FP for galaxy clusters, using the large data-sample from the ESO Nearby Abell Cluster Survey (ENACS, see Katgert et al. 1996, hereafter paper I, Mazure et al. 1996, hereafter paper II, Biviano et al. 1997, paper III, and Katgert et al. 1997, paper V), in combination with the Cosmos Galaxy Catalogue. As discussed in paper V, our Cosmos data contain parts of the well-calibrated Edinburgh-Durham Southern Galaxy Catalogue (EDSGC, Heydon-Dumbleton et al. 1989), as well as somewhat less well calibrated parts of the Cosmos catalogue outside the EDSGC (courtesy of H. McGillivray). Although in paper V we found evidence for a difference in the quality of the photometric calibration between the two kinds of Cosmos data, there was no evidence for systematic magnitude offsets between the two parts of the Cosmos Catalogue. So, for the present discussion we can regard the ENACS and Cosmos datasets to be both homogeneous.

In § 2 we give a short description of the sample of clusters that we used in the present analysis, and of the two catalogues. In § 3 we discuss the methods with which we determined the core-radii, R , the velocity dispersion, σ_v , and the total cluster luminosities, L . In § 4 we derive the parameters that describe the FP of galaxy clusters and in § 5 we compare our results to other determinations of the FP of galaxy clusters and early-type galaxies.

2. The data sample

The current work is based on a subsample of 29 clusters from the catalogue of Abell et al. (1989, ACO hereafter) with a redshift less than 0.1, for which at least 10 ENACS galaxy redshifts are available in the whole area. The typical redshift for these clusters is 0.07. We have selected those clusters for which galaxy b_j magnitudes and positions were available to us from the Cosmos catalogue, and we have limited the sample to clusters with very regular contours of projected galaxy density. In this way, we expect to reduce the scatter in the FP, due to the noise in the structural parameter measurements of clusters. In Fig. 1 we show surface density plots for two clusters (A0119 and A3111) which are representative for the total sample. For the other 27 clusters, contour plots will be given in paper VII.

We used the Cosmos data to calculate the integrated luminosity of the cluster galaxies in a given selected area, as well as to determine the characteristic scale of the cluster galaxy distribution. Note that the clusters A2734, A2764, A2799, A2800, A2911, A2923 and A3122 are in the EDSGC area around the Southern Galactic Pole, while the other 22 clusters are outside the EDSGC area but in the general Cosmos area. We assumed the entire Cosmos catalogue to have the same magnitude limit as the EDSGC subset, which is nearly complete at $b_j = 20$.

The ENACS dataset was used to obtain an estimate of the degree of background (or foreground) field galaxy contamination in the cluster area. The ENACS data also allow us to determine the cluster velocity dispersions. However, we cannot calculate the integrated luminosity from those data. Spectroscopy was attempted for galaxy samples with well-defined completeness limits in magnitude. However, as the spectroscopy has not yielded redshifts for all galaxies that were observed, the galaxies with redshifts do not define a truly magnitude-limited sample. In paper V we illustrate this by comparing the differential b_j magnitude distribution of the Cosmos galaxies to the differential R_{25} magnitude distribution of the ENACS galaxies, for each cluster separately. Since the two catalogues may cover different regions of each cluster (typically, the ENACS samples are restricted to the inner regions and rarely extend beyond $1.5 \text{ h}^{-1} \text{ Mpc}$), we have selected only the ENACS and Cosmos galaxies in the intersection of both surveys.

Absolute magnitudes are derived from apparent magnitudes using the cluster distance estimated from the mean cluster velocities, using a Hubble constant $H_0 = 100 \text{ km s}^{-1} \text{ Mpc}^{-1}$ and a deceleration parameter $q_0 = 0$. We scaled the R_{25} magnitudes to the b_j system by adopting a constant galaxy colour, $b_j - R_{25} = 1.5$ (see paper V). The Cosmos and ENACS magnitude distributions are quite similar down to a given limiting magnitude which corresponds to the (*a priori* unknown) magnitude completeness limit of the ENACS samples, which varies somewhat between clusters. If the Cosmos catalogue is complete to $b_j =$

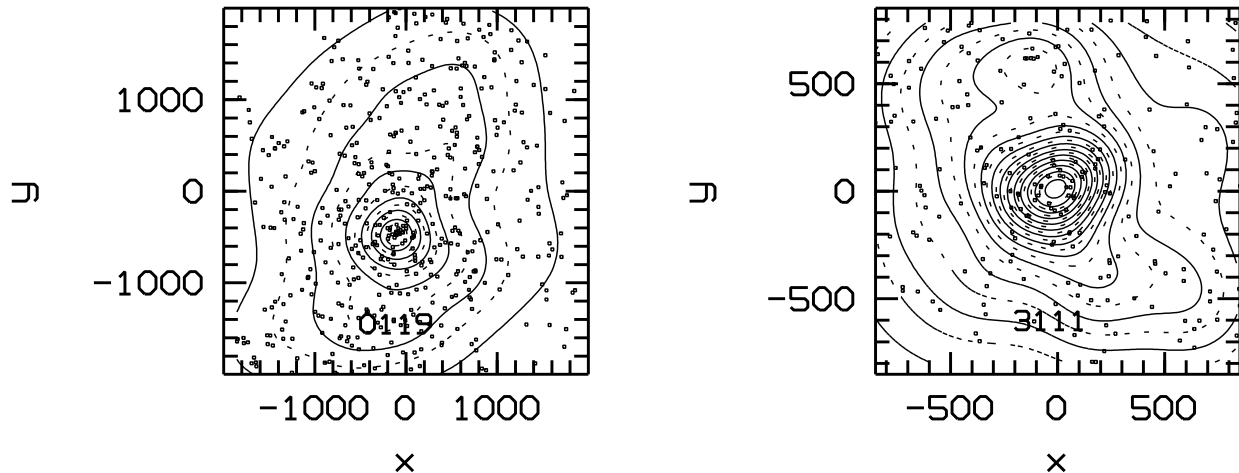


Fig. 1. Adaptive-Kernel maps of projected galaxy density for A0119 and A3111, from the Cosmos catalogue. Coordinates are in arcsec with respect to the geometric cluster center.

20, the ENACS catalogue is complete down to an absolute R_{25} magnitude of about -20.

3. Parameters of the Fundamental Plane

3.1. Characteristic Radii

Using Cosmos galaxy positions, we have fitted four kinds of density profiles to the galaxy distribution of each cluster. The background density is determined for each cluster and for each density profile. We used the profiles given by King (1962), by Hubble (e.g. Bruzual & Spinrad 1978), by de Vaucouleurs (1948) and by Navarro et al. (1996, which we will refer to as the NFW profile). These profiles were generalized by allowing the exponents to vary. Each profile has its characteristic scale, which we determined by Maximum Likelihood fitting (see paper VII for details). Although we used all four types of profile, it was found that only the King and Hubble profiles provide good fits to the observed clusters density profiles. The de Vaucouleurs and NFW profiles have cusps and do not provide a good fit to the projected galaxy density in the central regions of clusters, which do not show a significant central cusp. Therefore, we mostly use the characteristic radii of the King and Hubble profiles in the present discussion; these are listed (with their errors) in table 1.

As we need to adopt an area within which to define the cluster properties, we chose to consider a square of 10 core radii size centered on the cluster center assuming a King profile. The cluster center we adopted was determined it-

eratively by fitting a King profile. The centers of the clusters used in the present analysis are given in table 1. The chosen area is expected to include a large fraction of the true "physical cluster", as the galaxy volume density at 5 King core radii is about 1 % of the central density. For the other profiles the contrast between the central density and that at 5 King core radii is at least as large as for the King profile.

3.2. Velocity dispersions

The velocity dispersions were obtained from the ENACS data-base. All 29 clusters considered here have more than 10 galaxies in the selected area and in the main group identified in radial velocity space (see paper I). While in paper I the groups were defined using a fixed gap of 1000 km s^{-1} in radial velocity space, here we slightly modify this criterion to account for the fact that a fixed gap can overestimate the number of groups when the number density of galaxies is too low (simply because it is more likely to find larger gaps in sparse datasets). The new "variable" gap, which we will call *density gap*, is based on simulations of the occurrence of gaps of a given size in distributions of varying number of objects, drawn from the same Gaussian distribution. The density gap follows from the expression: $500 (1 + \exp(-(n-6)/33)) \text{ km s}^{-1}$, where n is the number of galaxies in the redshift survey of a given cluster.

Table 1. Data for the sample of 29 clusters. Col.(1) lists the cluster name, col.(2) the velocity dispersion, cols.(3) and (4) the King (K) and Hubble (H) radius, cols (5) and (6) N_{ENACS} and N_{Cosmos} , and cols (7) and (8) the fitted center of the clusters. In clusters marked by a † interlopers have been removed with the method of den Hartog & Katgert (1996).

Name	σ (km s ⁻¹)	R_c K(kpc)	R_c H(kpc)	N_{ENACS}	N_{Cosmos}	α (2000)	δ (2000)
A0013	1139±222	68±18	122±14	12	57	00:13:34.5	-19:29:38
A0087	510±107	118±12	263±51	21	81	00:43:00.7	-09:50:37
A0119 †	912±130	55±14	73±10	27	76	00:56:20.1	-01:15:51
A0151 †	911±159	56±9	94±16	20	81	01:08:50.1	-15:25:05
A0168 †	549±37	161±42	178±28	82	262	01:15:14.9	00:15:23
A0367	1096±145	128±21	162±26	19	84	02:36:35.2	-19:22:16
A0514 †	1187±107	90±25	117±33	31	106	04:48:15.1	-20:27:26
A1069	1002±96	219±65	411±65	32	202	10:39:47.9	-08:40:46
A2362	420±64	110±32	156±28	17	86	21:39:03.3	-14:21:10
A2480	805±190	101±28	272	10	68	22:46:10.7	-17:41:22
A2644	290±48	76±22	118±33	12	151	23:41:02.0	00:05:30
A2734 †	648±66	105 ±22	137	43	134	00:11:22.9	-28:50:55
A2764	949±122	101±22	126±25	14	133	00:20:29.5	-49:14:14
A2799	427±90	46±11	48±15	11	28	00:37:24.1	-39:09:01
A2800	461±49	98±25	87±26	19	71	00:37:58.7	-25:05:17
A2854	328±118	66±17	70±11	10	49	01:00:47.2	-50:32:38
A2911	513±121	109±28		21	130	01:26:08.0	-37:57:26
A2923	401±87	142±19	96±19	14	47	01:32:28.8	-31:04:41
A3111	761±281	99±26	180±23	22	98	03:17:49.0	-45:43:38
A3112 †	865±222	229±29	433±65	69	403	03:17:58.5	-44:14:21
A3122 †	898±76	149±20	319	53	218	03:22:14.0	-41:19:14
A3128 †	895±60	362±29	520±39	123	867	03:30:37.9	-52:31:51
A3141	758±124	176±51		13	92	03:36:54.3	-28:04:20
A3158 †	1310±123	101±15	104±12	35	205	03:43:04.6	-53:38:40
A3202	485±82	64±20	132±39	12	51	04:00:55.5	-53:41:17
A3733	768±249	37±11	84±15	10	44	21:01:34.7	-28:02:42
A3764	829±130	60±16	97±12	12	45	21:25:47.3	-34:42:44
A3825 †	947±87	108±16	227±50	27	141	21:58:26.0	-60:22:03
A3827	962±407	57±29	102±13	11	99	22:01:52.0	-59:56:42

We stress that the criterion used in paper I works very well for the ENACS datasets, since the number of galaxies does not vary too much. However, when we consider cluster datasets drawn from the literature, large differences in the number densities may occur. This is the case when one includes, e.g., the Virgo or the Coma clusters, for which redshifts are known for more than 500 galaxies. In these cases a fixed gap-size fails to identify the main cluster structure, and merges systems which are likely to be separate entities. For the present paper, we could have maintained the fixed gap definition, but since we will in the future also include large datasets such as that of Coma, we prefer to use the density gap already in this discussion. We stress that using this gap definition, the membership of the ENACS main systems hardly changes, compared to paper I.

Similarly to what we did in paper II, we identified interlopers in the systems by using both the spatial and the velocity information. More specifically, we applied the technique developed by den Hartog and Katgert (1996) to

clusters with at least 50 galaxies left after the gapping in velocity space. These clusters are marked in table 1. The effect of the interloper removal was discussed at length in paper II. For systems with less than 50 galaxies the method becomes unreliable so we have not applied interloper rejection to these systems.

For the clusters thus defined, we calculate the velocity dispersion by a biweight technique using the ROSTAT package (Beers et al. 1990), which is ideally suited for poorly sampled and/or non-Gaussian distributions. As it is difficult to say whether our velocity distributions are truly Gaussian (in some cases we only have 10 galaxies), a classical velocity dispersion estimator might not give a reliable value. Lax (1985) has shown, from simulations, that the biweight estimator gives better results in that case. Errors were estimated from 1000 bootstrap resamplings for each cluster (see Stein 1996).

The reliability of our velocity dispersion values can be checked by a comparison with previous investigations. In paper II we obtained velocity dispersions by using a fixed

gap criterion, and using all galaxies in the ENACS regions. The present velocity dispersion estimates were correlated with those in paper II, and the best-fit straight line has a slope of 0.98 ± 0.15 and an offset of 113 ± 130 , clearly consistent with a slope of 1 and an offset of 0. Comparing the present velocity dispersions with those of Fadda et al. (1996), who used a combination of ENACS and literature data, we find a best-fit line with a slope of 0.90 ± 0.17 and an offset of 235 ± 203 , which again is consistent with the hypothesis that the two estimates are equivalent.

3.3. Luminosity

In order to determine the cluster luminosities, we used the Cosmos data, and followed the procedure described below.

1. We summed up the individual apparent luminosities of all galaxies in the selected area, after K-correcting the Cosmos b_j magnitudes following Frei & Gunn (1994) and assuming that all galaxies lie at the average redshift of the main system (as determined from the ENACS data). We then converted from apparent to absolute magnitudes (using the standard cosmological formulae, see, e.g. Lang 1980), assuming an M_{B_j} solar magnitude of 5.53 (Lang, 1980, Gullixson et al. 1995). The result is L_{Cosmos} .
2. We applied a correction to the integrated luminosities for the contamination by fore- and background galaxies, by making the assumption that the fraction $C_1 = 1 - (L_{fore+background})/L_{tot}$ of the luminosity of cluster galaxies in the selected field, is the same in the Cosmos sample as it is in the ENACS sample, i.e. assuming that $C_1 = C_{Cosmos} = C_{ENACS}$. This is only approximately true, because this fraction changes with limiting magnitude and the Cosmos limit is 0.5 to 1.0 magnitude fainter than the ENACS limit. However, for some clusters that were very well sampled in the ENACS data we have verified that C_1 is not significantly biased.

This allows us to take advantage of the fact that all ENACS galaxies have a measured redshift, so that membership assignment is relatively straightforward (while of course many Cosmos galaxies do not have such information available). We can then separate the luminosity of the cluster members from that of fore- and background galaxies. We calculate the value of C_{ENACS} for each cluster, which we assume to be equal to C_1 . We find the mean value of $C_1 = 0.83$ if we consider only clusters with more than 15 galaxies. For the clusters with relatively poor statistics, the individual corrections are not considered reliable. Therefore, we apply the mean correction to all clusters by taking the mean value $\langle C_1 \rangle = 0.83$; this introduces an uncertainty in the luminosities of the order of the dispersion in the C_1 values, which is 0.10. We thus have:

$$L_1 = \langle C_1 \rangle \times L_{Cosmos}$$

3. We correct for the incompleteness effect due to the Cosmos magnitude limit as follows. We adopt a completeness magnitude for the Cosmos catalogue of $b_j = 20$. Following Ellis et al. (1996), we take into account all fainter cluster members by adopting the following Schechter (1976) luminosity function:

$$\varphi(L) = \left(\frac{L}{L^*}\right)^{\alpha_S} e^{-\frac{L}{L^*}}$$

with $\alpha_S = -1.1$, $M_{b_j}^* = -18.8$ and L the absolute luminosity.

The fraction of the total luminosity that we have observed is then equal to:

$$F = \frac{\int_{L_{lim}}^{+\infty} L\varphi(L)dL}{\int_0^{+\infty} L\varphi(L)dL}$$

where the value of L_{lim} follows for each cluster from the median redshift and $b_{j,lim} = 20$. Finally we have:

$$L_2 = C_2 \times L_1 = L_1/F.$$

We have checked the dependence of C_2 on α_S . For the same limiting magnitude and a redshift equal to 0.07 (the typical distance of our clusters), we have a variation of less than 10% of C_2 when α is changed from 0.5 to 1.3. There is thus only a weak dependence of the total luminosity on α when this parameter is in the commonly employed range of values (e.g. Carlberg et al. 1996, Lumsden et al. 1997).

4. There is an additional source of incompleteness at bright luminosities. In fact, we have found that in some cases, bright ENACS galaxies have no Cosmos counterpart (see paper V). In those cases, we simply add C_3 , i.e. the sum of the ENACS luminosity (scaled to the b_j system) of the galaxies which inadvertently were not included in L_{Cosmos} :

$$L_3 = L_2 + C_3.$$

5. Finally, we correct for galactic extinction A_{b_j} by using the Burstein & Heiles map (1982). We use the formula $A_{b_j} = 4.25 \times E(B - V)$. The correction to the luminosity is $C_4 = 10^{0.4 \times A_{b_j}}$. We have:

$$L_{true} = L_3 \times C_4.$$

All individual corrections are given in table 2; note however that the values of C_1 are given for information only, as we applied $\langle C_1 \rangle = 0.83$ for all clusters.

Estimating the errors on the luminosities L_{true} is not easy. From the uncertainty in the slope of the luminosity function, we estimate that L_{true} is uncertain by 10 %. To this we should probably add other error sources but it is very difficult to make quantitative estimates of those. Therefore we take the optimistic view of an error of 10 % in the luminosities.

To check the general consistency of our luminosities, we compare them with those obtained by Carlberg et al. (1996). They found, in Gunn r, a median K-corrected luminosity for 16 distant ($z \approx 0.3$) clusters of $1.95 \cdot 10^{12} h^{-2} L_{\odot,r}$, corresponding, to a value of $9.36 \cdot 10^{11} h^{-2} L_{\odot,b_j}$, where we assumed $b_j - r = 1.5$ and $b_{j\odot} - r_{\odot} = 0.7$. Our mean cluster luminosity is $7.65 \cdot 10^{11} h^{-2} L_{\odot,b_j}$. Given that Carlberg et al. (1996) considered larger areas than

Table 2. Luminosities (in units of $h^{-2}L_{b_j,\odot}$) and corrections for the 29 clusters.

Name	L_{true}	C_1	C_2	C_3	C_4
A0013	$5.90 \cdot 10^{11}$	1.00	1.35	0.	1.00
A0087	$2.48 \cdot 10^{11}$	0.70	1.12	$1.7 \cdot 10^{10}$	1.10
A0119	$3.14 \cdot 10^{11}$	0.86	1.08	$8.8 \cdot 10^{10}$	1.12
A0151	$3.82 \cdot 10^{11}$	1.00	1.11	$1.6 \cdot 10^{10}$	1.00
A0168	$6.20 \cdot 10^{11}$	1.00	1.08	$6.9 \cdot 10^{10}$	1.00
A0367	$7.90 \cdot 10^{11}$	1.00	1.32	0.	1.06
A0514	$5.09 \cdot 10^{11}$	0.85	1.20	$2.5 \cdot 10^{10}$	1.04
A1069	$9.27 \cdot 10^{11}$	0.95	1.16	0.	1.08
A2362	$2.68 \cdot 10^{11}$	0.60	1.15	$1.9 \cdot 10^{10}$	1.12
A2480	$3.46 \cdot 10^{11}$	0.74	1.20	0.	1.09
A2644	$5.72 \cdot 10^{11}$	1.00	1.19	$1.5 \cdot 10^{10}$	1.09
A2734	$5.31 \cdot 10^{11}$	0.74	1.15	$9.7 \cdot 10^{10}$	1.00
A2764	$7.69 \cdot 10^{11}$	0.77	1.19	0.	1.00
A2799	$1.30 \cdot 10^{11}$	1.00	1.15	$6.0 \cdot 10^{10}$	1.00
A2800	$3.35 \cdot 10^{11}$	0.74	1.16	$1.9 \cdot 10^{10}$	1.00
A2854	$2.19 \cdot 10^{11}$	1.00	1.14	$5.7 \cdot 10^{10}$	1.00
A2911	$8.41 \cdot 10^{11}$	0.88	1.25	0.	1.00
A2923	$3.78 \cdot 10^{11}$	0.81	1.19	$1.04 \cdot 10^{11}$	1.00
A3111	$8.01 \cdot 10^{11}$	0.75	1.24	0.	1.00
A3112	$2.424 \cdot 10^{12}$	0.87	1.22	0.	1.00
A3122	$6.65 \cdot 10^{11}$	0.81	1.16	$9.8 \cdot 10^{10}$	1.00
A3128	$3.812 \cdot 10^{12}$	0.89	1.14	$5.4 \cdot 10^{10}$	1.00
A3141	$1.311 \cdot 10^{12}$	1.00	1.44	0.	1.00
A3158	$9.71 \cdot 10^{11}$	1.00	1.14	$1.48 \cdot 10^{11}$	1.00
A3202	$2.71 \cdot 10^{11}$	0.66	1.19	$1.0 \cdot 10^{10}$	1.00
A3733	$1.26 \cdot 10^{11}$	1.00	1.06	$2.6 \cdot 10^{10}$	1.42
A3764	$3.23 \cdot 10^{11}$	0.82	1.23	$3.3 \cdot 10^{10}$	1.21
A3825	$2.208 \cdot 10^{12}$	0.90	1.22	$3.3 \cdot 10^{10}$	1.02
A3827	$8.96 \cdot 10^{11}$	1.00	1.38	$4.4 \cdot 10^{10}$	1.02

we do (larger than $1.0 h^{-1}$ Mpc vs. $0.9 h^{-1}$ Mpc), the agreement can be considered quite satisfactory.

4. The Fundamental Plane

As discussed in § 2, we want to investigate possible L - R - σ correlations for the galaxy clusters in our sample. In the process, we also look at possible L - R , L - σ and R - σ relations. Note that all fits were performed on the sample of the 20 most contrasted clusters (see below). The cluster A0168 is the only one we have in common with S93.

4.1. Fitting techniques

We employ three fitting methods. First, we used the ESO MIDAS-package which has an integrated fitting procedure that we used with and without weights. The method consists of a classical least squares fit, either unweighted, or weighted by the inverse of the square of the error in velocity dispersion or characteristic radius.

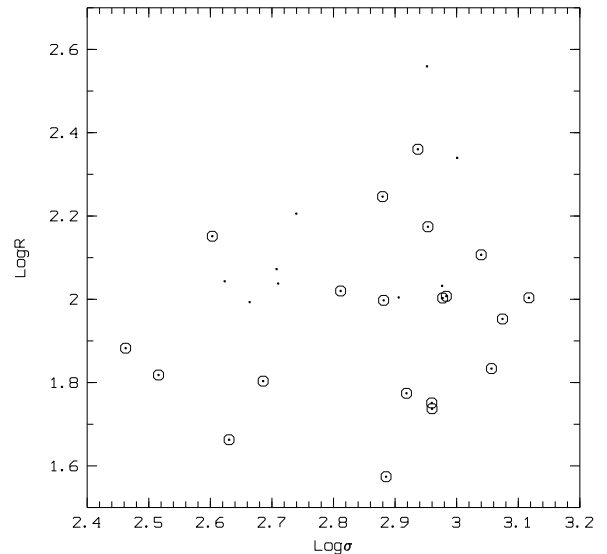


Fig. 2. R - σ relation for King profile fits. The dotted circles represent the more contrasted clusters while the dots denote the less contrasted ones.

We also used the MINUIT package to do a least squares fitting by minimizing χ^2 . This method has been developed to fit particle trajectories and it is recognized to provide very good results. The two MINUIT minimization methods are Simplex (Nelder et al. 1965) and Migrad (Fletcher,1970). These two methods do not use derivatives. Our strategy was to use Simplex to approach the final parameter values and Migrad to solve for the parameters and estimate their errors. As we show in paper VII, Simplex systematically underestimates the errors. If Migrad does not converge, we take only the Simplex values without errors. The strategy of using Migrad after Simplex in practice gives good results and is commonly used, for example in the minimization routines of the Greg numerical package.

4.2. Results of the fitting

We performed the fitting of σ_V vs. R only on the subsample of the 20 more contrasted clusters in order to avoid contaminating our sample with uncertain values of velocity dispersion. The contrast is defined as the percentage of all galaxies in the selected area which are cluster members. The number of background galaxies was deduced from the background density calculated by fitting the theoretical profiles (paper VII). The nine less contrasted clusters excluded from the fitting analysis are A0087, A0168, A1069, A2362, A2480, A2800, A2911, A3128 and A3825.

The clusters are indicated in Figs. 3, 4 and 5 by dots and dotted circles, to distinguish the 9 less contrasted from the 20 more contrasted clusters.

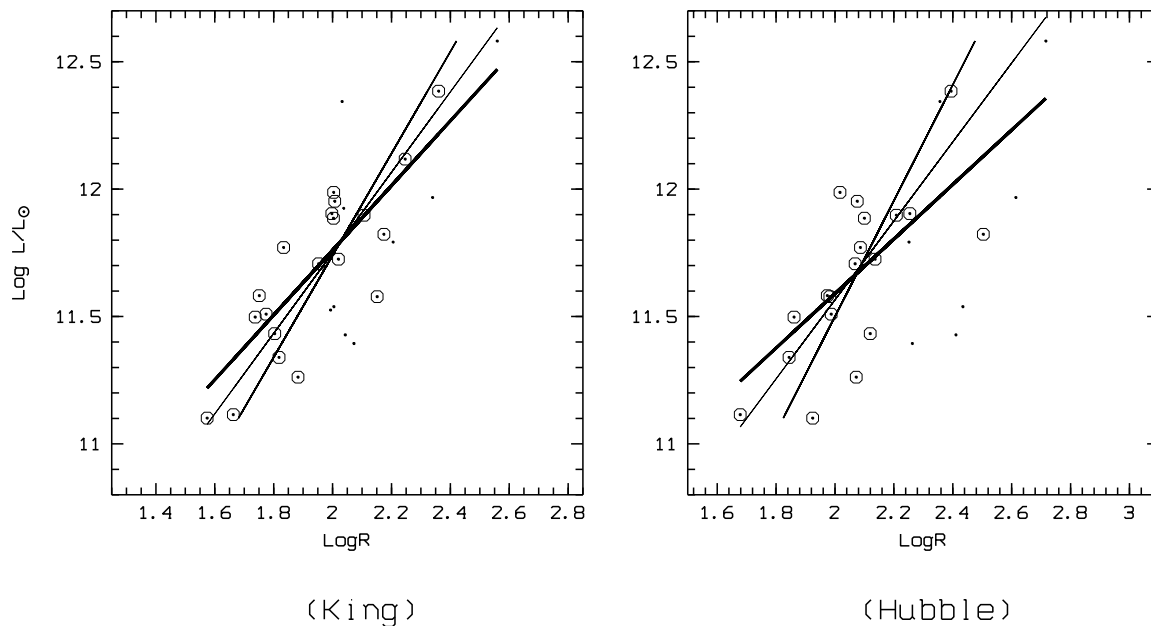


Fig. 3. L - R relation for King (left) and Hubble (right) profiles (MIDWW calculations). The dotted circles represent the more contrasted clusters and the dots are the less contrasted clusters. The heavy line is the L - R relation, the intermediate line the R - L relation and the thin line is the bisector relation, which has a slope of 1.58 for the King profile and 1.55 for the Hubble profile.

We checked for the existence of a relation between σ_v and R , where we considered only King and Hubble radii, as discussed in Sec 3. None of the various fitting routines finds a relation between radius and velocity dispersion (see e.g. Fig. 2, for King profile fits), in agreement with the conclusion of Girardi et al. (1996).

On the other hand, R and L are correlated. The fitting of the L vs. R (and R vs. L) relations was done using two MIDAS regressions, viz. with (hereafter MIDWW) and without (hereafter MIDWOUTW) weights on the fitted quantities. The fits were also made using MINUIT (hereafter MWOUTW), without assigning any weight to the data. Results of the fits are given in Table 3, where the parameters α_1 , cst_1 , α_2 and cst_2 are defined by: $(L/L_\odot) = (R/kpc)^{\alpha_1} * 10^{cst_1}$ and $(R/kpc) = (L/L_\odot)^{\alpha_2} * 10^{cst_2}$. Note that only the King and Hubble radii were considered. The weight that we used here is the inverse of the square of the uncertainty in the R -determination. Fig. 3 shows the R vs. L scatter plots. In addition to the data, we also show the fitted L - R and R - L relations, as well as the bisector line which is the best estimator of a linear

relation between two parameters, according to Isobe et al. (1990).

Table 3. Fitted parameters for the two types of characteristic radius and the three fitting methods, for the L - R relation.

parameters	MWOUTW	MIDWW	MIDWOUTW
α_1 (King)	1.38 ± 0.24	1.27 ± 0.23	1.39 ± 0.20
cst_1 (King)	8.98 ± 0.24	9.22 ± 0.46	8.98 ± 0.18
α_2 (King)	0.51 ± 0.12	0.50 ± 0.09	0.51 ± 0.08
cst_2 (King)	-4.02 ± 0.13	-3.87 ± 0.10	-4.06 ± 0.11
α_1 (Hubble)	1.22 ± 0.18	1.07 ± 0.27	1.22 ± 0.29
cst_1 (Hubble)	9.12 ± 0.21	9.50 ± 0.58	9.12 ± 0.23
α_2 (Hubble)	0.42 ± 0.09	0.44 ± 0.11	0.42 ± 0.10
cst_2 (Hubble)	-2.78 ± 0.17	-3.11 ± 0.33	-2.78 ± 0.14

A correlation is also found between σ and L . We fitted the parameters γ_1 , cst_1 , γ_2 and cst_2 in the relations

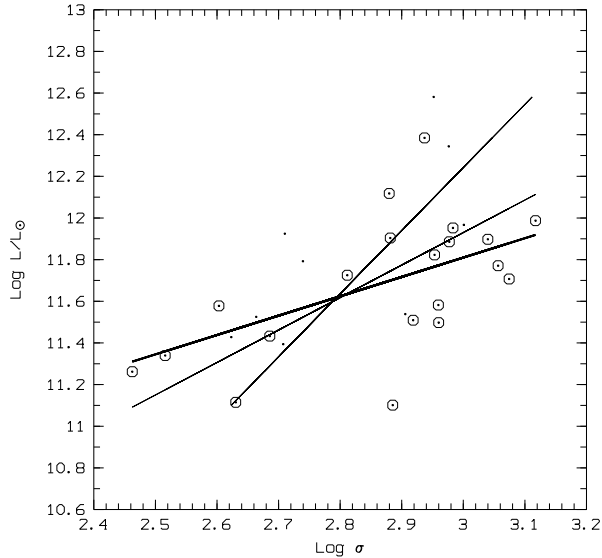


Fig. 4. The L - σ relation (MIDWW calculations). The dotted circles represent the more contrasted clusters and the dots the less contrasted ones. The heavy line is the L - σ relation, the intermediate line the σ - L relation and the thin line the bisector relation which has a slope of 1.56.

$(L/L_{\odot}) = \sigma^{\gamma_1} * 10^{cst1}$ and $\sigma = (L/L_{\odot})^{\gamma_2} * 10^{cst2}$ (see Tab. 4 and Fig. 4), with σ in km s^{-1} . The weight that we used here is the inverse of the square of the uncertainty in the σ -determination.

Table 4. Fitted parameters for the two types of characteristic radius and the three fitting methods, for the L - σ relation.

parameters	MWOUTW	MIDWW	MIDWOUTW
γ_1	1.04 ± 0.32	0.93 ± 0.27	1.04 ± 0.33
cst1	8.69 ± 0.29	9.02 ± 0.80	8.67 ± 0.28
γ_2	0.33 ± 0.13	0.33 ± 0.11	0.33 ± 0.11
cst2	-1.04 ± 0.15	-1.04 ± 1.20	-1.04 ± 0.16

Finally we fitted the parameters α and β in the relation $(L/L_{\odot}) = R^{\alpha} \sigma^{\beta} * 10^{cst}$, with R in kpc and σ in km s^{-1} , for both the King and Hubble radii (see Fig. 5 and Tab. 5). We have made a fit which minimizes the r.m.s. deviation in the L direction. The weight used in the MIDWW regression is the inverse of the square of the error in R . From Fig. 5 one can see that the less contrasted clusters have a slightly larger dispersion around the fit than the more contrasted ones. We have verified that the parameters and the dispersion around the fit do not vary significantly if we slightly change the area in which we calculate the luminosity. In addition, the dispersion in the L - R - σ relation

for the King radius with a luminosity calculated within 4 King radii instead of 5, is smaller than when the luminosity is calculated within 4 Hubble radii.

Table 5. Fitted parameters for the two types of characteristic radius and the three fitting methods, for the L - R - σ relation.

parameters	MWOUTW	MIDWW	MIDWOUTW
α (King)	1.24 ± 0.12	1.19 ± 0.14	1.25 ± 0.13
β (King)	0.78 ± 0.15	0.91 ± 0.16	0.78 ± 0.14
cst (King)	7.00 ± 0.13	6.74 ± 0.51	7.00 ± 0.11
α (Hubble)	0.98 ± 0.09	0.87 ± 0.26	0.98 ± 0.26
β (Hubble)	0.71 ± 0.11	0.70 ± 0.31	0.71 ± 0.26
cst (Hubble)	7.60 ± 0.25	7.92 ± 0.86	7.60 ± 0.20

Following Jørgensen et al. (1996), we have also minimized the r.m.s. deviations in the two other directions (Table 6). We ran only a MIDWW fit for the King profile. We find no significant variations with minimization direction. This supports the reliability of our fitting results.

The differences between the values of the parameters obtained with different methods are within the fitting errors. There is a slight apparent inconsistency in the results of the 2-parameter fits when minimized in the two parameter directions. For example, the slope γ_1 and the slope γ_2 in the relation between luminosity and velocity dispersion certainly do not obey $\gamma_1 \approx \frac{1}{\gamma_2}$. However, it is well known that one has $\gamma_1 = \frac{1}{\gamma_2}$ only if the correlation coefficient between L and σ is 1. In other words, one must have the same covariance between L and σ as between σ and L which is clearly not the case. On the other hand, the coefficients of the L - R - σ relations do not depend significantly on the minimization direction. The dispersion in the 3-parameter relation is smaller than in the two 2-parameter relations, and the correlation coefficient is close to unity.

Table 6. Fitted parameters for the cluster L - R - σ relation, for the three minimization directions, using the King radius

direction	$(L \propto R^{\alpha} \sigma^{\beta})$	
	α	β
L	1.19 ± 0.14	0.91 ± 0.16
R	1.43 ± 0.14	0.87 ± 0.32
σ	1.37 ± 0.21	1.15 ± 0.38

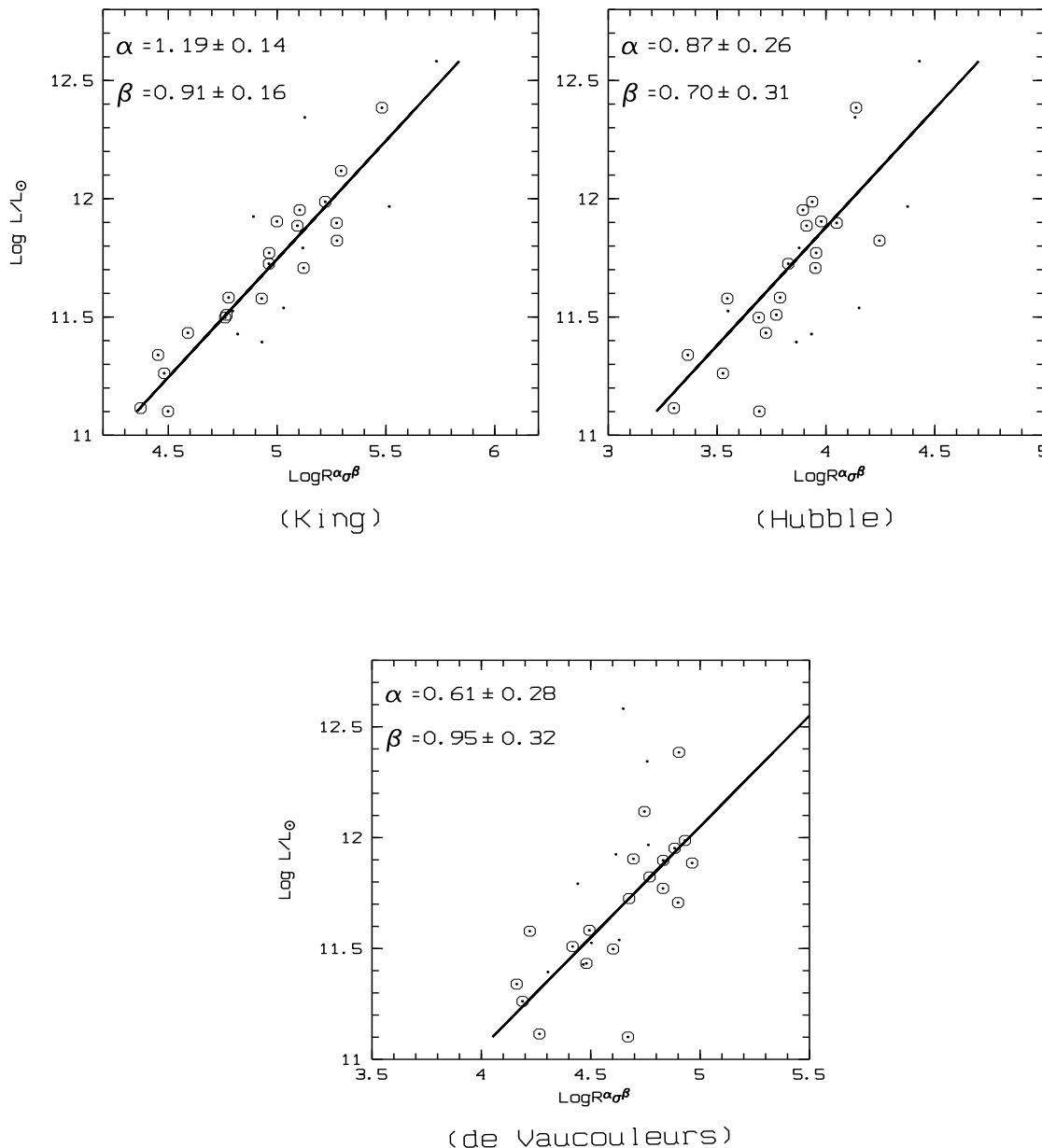


Fig. 5. L - R - σ relation for King, Hubble and de Vaucouleurs profiles (MIDWW calculations). The dotted circles represent the more contrasted clusters and the dots are the less contrasted ones. The abscissa is equal to the logarithm of $R^\alpha \sigma^\beta$.

5. Discussion

We have confirmed the result of Schaeffer et al. (1993) that clusters of galaxies populate a Fundamental Plane (FP). The orientation of the FP of clusters can be determined reasonably well from our ENACS data, but the details depend somewhat on the ‘direction’ in which we minimize the r.m.s. deviations from the FP. In particular, we find a slightly steeper dependence of L on σ if we minimize in the

σ -direction, although the difference is not significant. In Fig. 5 we show what is essentially a sideways view of the FP by projecting the observations in a direction parallel to the FP, onto a plane that is orthogonal to the FP. The reality of the inclination of the FP in the $(\log L, \log R, \log \sigma)$ -space is evident already in Figs. 2, 3 and 4, which represent projections along the coordinate axes. In Fig. 6 we show an attempt at a 3-dimensional visualisation of

the FP in the $(\log L, \log R, \log \sigma)$ -space. This figure is for King profile fits.

The comparison with the FP parameters obtained by S93, for a different sample of clusters, requires some care because S93 used a de Vaucouleurs profile fit. Therefore, we have also repeated our analysis for de Vaucouleurs-profile fits for our clusters. However, we stress once again that this profile provides a fit to the data that is inferior to that of a King or Hubble profile (see also paper VII).

In Tab. 7 we give the FP parameters obtained from the ENACS clusters for the 3 types of profile just mentioned. Although the effect is not highly significant in view of the errors, there is a tendency for the L-dependence on R to decrease from King to Hubble to de Vaucouleurs profile. However, there is no apparent change of the dependence of L on σ along the same sequence. We also show in the same table the FP parameters derived by S93. There is a hint that the relation between L and σ_v (for the de Vaucouleurs profile) may be steeper in S93 than it is in our data, but the difference of about 30% in β is within one sigma. It is therefore evident that the present results qualitatively agree well with those of S93, although there are some quantitative differences. This provides additional evidence of the reality of the galaxy cluster FP, because both the data-samples and the methods used are different.

We note in passing that West et al. (1989) derived an L - R relation, using the same data as S93, that also agrees quite well with our result.

For clusters in virial equilibrium, which have a fixed value of M/L , one expects $L \propto R\sigma^2$, i.e. $\alpha = 1.0$ and $\beta = 2.0$. Clearly, our β -value is different from the virial prediction. In this respect, there is a similarity between galaxy clusters and elliptical galaxies. The deviation from the pure virial relation, as apparent from the cluster FP, may not seem very large but it is quite significant. This is apparent from the orthogonal dispersion of the 20 clusters around the virial relation of 0.12, which is more than two times larger than the dispersion around our best-fitting FP of 0.05 (see also Table 8). For the sake of the present discussion, we will therefore assume that the FP-fit to our data provides a considerably better description of the $L - R - \sigma$ -relation of galaxy clusters than does the virial relation.

The virial theorem can be expressed as follows (Kormendy & Djorgovski, 1989):

$$L = S R_d \frac{L}{M} R \sigma_v^2$$

In this equation, S is a parameter related to the internal structure of the system, and R_d is the ratio of the potential to the kinetic energy of the system, and it measures the degree of relaxation of the system. The deviations of the (α, β) coefficients from the (1,2) virial prediction could be the result of a non-constant value for the product of S , R_d and M/L for the different clusters.

As discussed in S93, the case of non-constant M/L has a special solution if $\frac{M}{L} \propto L^\epsilon$; then one has $\beta = 2\alpha$. For the FP fit in S93, with $\alpha = 0.89 \pm 0.15$ and $\beta = 1.28 \pm 0.22$, this

special case could indeed apply. If we take our result for de Vaucouleurs fits to the density profiles ($\alpha = 0.61 \pm 0.28$ and $\beta = 0.95 \pm 0.32$) we would again conclude that the data are consistent with this special case. However, we must stress again that the de Vaucouleurs profile fits are notably worse than the King profile fits. Comparing therefore the values $\alpha = 1.19 \pm 0.20$ and $\beta = 0.91 \pm 0.26$ that we found for the King profile fits, we conclude that M/L is likely not to have a simple power-law dependence on L .

This would then imply that probably also different S and R_d are needed for different clusters to explain the deviation of the cluster FP from the virial relation. Another way to summarize the situation could be to say that the structure of clusters is such that the simple equilibrium density laws *either* do not fit the data very well (de Vaucouleurs), while M/L can be assumed proportional to L or M , *or* they fit quite nicely (King) but then it is unlikely that M/L has a simple power-law dependence on M .

We can set an upper limit to the variation of M/L among clusters, if we assume the virialization state and internal structure of all clusters to be identical. In that case $M/L \propto R^{1-\alpha} \sigma_v^{2-\beta}$, or approximately $M/L \propto \sigma_v^{2-\beta}$ because $\alpha \approx 1$. I.e., systems with larger σ_v have larger M/L . The M/L ratio of rich clusters would then be expected to vary at most a factor of 2 to 3, given the observed σ_v -range of rich galaxy clusters (see paper II).

If the M/L ratio of rich clusters indeed is more or less proportional to σ_v , this could fundamentally affect the determination of the density parameter of the Universe from clusters which are acting as gravitational lenses. These clusters are generally among the most massive ones so they have a large σ_v . Therefore they could have atypically high M/L ratios which would lead to an overestimation of the density parameter (e.g. Bonnet et al. 1994).

It is of interest to compare the cluster FP with that of elliptical galaxies. The results of Djorgovski & Davis (1987), Bender et al. (1992), Guzman et al. (1993), Pahre et al. (1995) and Jørgensen et al. (1996), are listed in Tab. 7. As was done by Jørgensen et al. we translated, if necessary, the published FP solution to the form we used ($L \propto R^\alpha \sigma^\beta$) by using the relation: $\langle I_e \rangle \propto L/r_e^2$. Of course, this is not exactly identical as we determined L , σ and R independently, whereas r_e and $\langle I_e \rangle$ were derived from the same luminosity profile, and are therefore somewhat correlated. We have also used the global, overall velocity dispersion, while for ellipticals it is the central velocity dispersion that is used. However, the velocity dispersion profiles of galaxy clusters are in general quite flat (see e.g. den Hartog and Katgert 1996). Note that the result of Pahre et al. refers to the near-infrared, while the other results refer to the optical.

The α -values found for ellipticals by the various authors, in the optical and near-infrared, appear quite consistent. The β -values found by the different groups are also quite similar, although the value found in the near-infrared (Pahre et al., 1995) is slightly high compared to

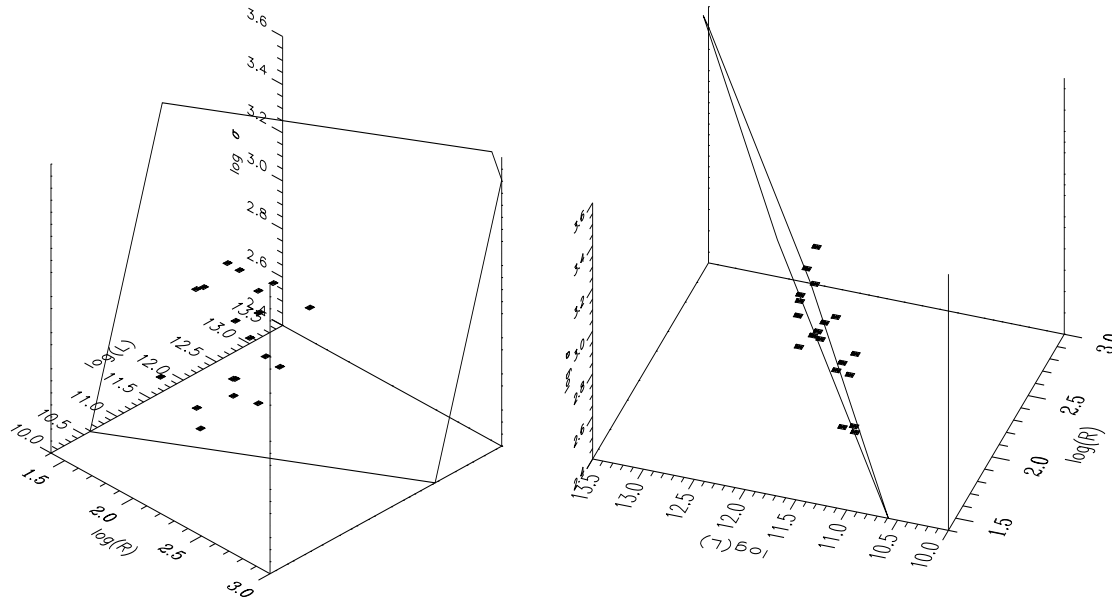


Fig. 6. Two projections of the Fundamental Plane of clusters, in the $(\log L, \log \sigma, \log R)$ -space, which show the distribution of clusters in the plane (left) and the dispersion around the plane (right).

Table 7. Fundamental Plane parameters for galaxy clusters and for elliptical galaxies.

Authors	Type of system	α	β
present paper	galaxy clusters (King profile)	1.19 ± 0.14	0.91 ± 0.16
present paper	galaxy clusters (Hubble profile)	0.87 ± 0.26	0.70 ± 0.31
present paper	galaxy clusters (de Vaucouleurs profile)	0.61 ± 0.28	0.95 ± 0.32
Schaeffer et al.	galaxy clusters (de Vaucouleurs profile)	0.89 ± 0.15	1.28 ± 0.22
Djorgovski & Davis	Virgo ellipticals	0.89	1.54
Bender et al.	cluster ellipticals	0.82	1.64
Guzman et al.	cluster ellipticals	0.72	1.44
Pahre et al. (1995)	cluster ellipticals	0.73 ± 0.07	1.82 ± 0.14
Jørgensen et al.	Coma ellipticals	0.78 ± 0.05	1.51 ± 0.09

the optical values. This is even more evident in the recent result by Pahre et al. (1996) who find, again in the near-infrared, $\alpha = 0.67$ and $\beta = 2.21$.

Comparing the various determinations of α and β in Tab. 7, we cannot be certain that the values of α are significantly different for ellipticals and for galaxy clusters. This does not mean that they are identical. As we said before, the agreement in α is good for de Vaucouleurs fits to the cluster profiles, but much less (about 2σ) for the King profile that describes our cluster observations much better. The situation appears much clearer for β : independently of the type of profile used, the β -value for the clusters appears significantly lower ($\geq 2\sigma$) than that of

the ellipticals and much more when compared to the result described by Pahre (1996).

With caveats of the previous paragraphs in mind, it seems safe to conclude from Tab. 7 that the FP's of clusters of galaxies and of elliptical galaxies have different orientations. It is therefore quite unlikely that the two types of system share a common, universal FP, and we do not think that our data support the conclusion to this effect in S93. If our result is confirmed, this will have very important implications for the formation of gravitationally bound systems on different scales. A more accurate determination of the cluster FP is needed in order to quantify the differences between the FP's of galaxy clusters and of

elliptical galaxies more accurately before one can start to investigate the implications in more detail.

For the moment, we can only speculate about the possible implications. Taking the values in Tab. 7 at face value, we are struck by the fact that the deviations from the virial prediction seem to be different for galaxy clusters and ellipticals. For the ellipticals it seems that the value of β may be quite close to the virial value (especially in the near-infrared). Or, if one gives more weight to the optical data, the ellipticals at least seem to obey the relation $\beta = 2\alpha$ quite well. None of that is true for the clusters, for which it seems quite likely that α agrees with the virial prediction (which probably is not the case for ellipticals!), while the value of β seems definitely at odds with the virial expectation.

Therefore, it is possible (if not likely) that the deviations from the virial prediction have quite different origins for ellipticals and for clusters. For ellipticals the deviations may well be due to non-homology and non-constant M/L ratio's. For clusters the deviations may be due primarily to their relative youth or, in other words: to an absence of real equilibrium. Even though we selected the most regular and apparently relaxed clusters for the present analysis, it is unlikely that they have really attained equilibrium except in their very centres (see e.g. den Hartog and Katgert 1996, and paper III). If this is true, it is not immediately clear why we should still find a well-defined FP for these clusters which probably are not fully relaxed.

The orthogonal dispersion of the 20 well-contrasted clusters around the FP that they define is 0.05. This is supported by visual inspection of the upper left-hand panel of Fig. 5. However, inspection of that same figure also reminds one of the fact that the other 10 clusters are distributed less narrowly around the FP. For the moment we will assume that these less contrasted and less regular clusters are probably not as relaxed as the other 20 clusters, so that one cannot expect them to define an FP as narrowly as the more contrasted and more regular clusters. It is interesting to observe in Fig. 5 that the dispersion around the FP is indeed smallest for the King profile, somewhat larger for the Hubble profile and largest for the de Vaucouleurs profile. This supports in a rather independent way the conclusion in paper VII that de Vaucouleurs profiles do not provide good fits to the galaxy distributions in clusters.

We have tried to estimate how much of the scatter in the FP is due to measurement errors and how much to the intrinsic width of the FP. To that end we have done the following experiment. We have assumed the solution for the FP, with $\alpha = 1.19$ and $\beta = 0.91$, to be correct. Therefore, we have taken the orthogonal projections of the observed points onto that FP as starting points for the following simulations. For the set of 20 points *in the FP* obtained thus, we simulated 500 artificial sets in which uncorrelated errors are added in L , R and σ to each of the 20 points, according to Gaussian distributions with

dispersions as given in Tab. 1 and section 3.3. We assumed an error of 10% for L .

For each of the 500 sets of 20 artificial points, the FP was solved in exactly the same way as it was done for the observations with the MIDWW method. As a result we obtain 500 pairs (α, β) . The distributions of the 500 values of α and β yield average values and dispersions of 1.17 ± 0.06 and 0.96 ± 0.10 for α and β respectively. These values must be compared to the values and their estimated errors from the FP fit to the observations of 1.19 ± 0.14 and 0.91 ± 0.16 . The estimated errors in the latter values are calculated from the assumed errors in L , R and σ .

The average values of α and β in the 500 artificial sets are not identical to the input values (the most probable values found in the FP fit to the data) but they are quite close. On the other hand, the dispersions in the α and β values of the 500 artificial sets are significantly smaller than the estimated uncertainties found in the FP fit to the data. We interpret this as evidence that the apparent width of the FP of 0.05 (for the King profile fits) has a important contribution from the intrinsic width of the FP, i.e. that it is not exclusively due to measurement errors.

It is not trivial to estimate how much of the apparent width of the observed FP is intrinsic. One can get some idea from the average dispersion around the 500 artificial datasets of 20 'observed' points, generated as described above. The average dispersion around these 500 individual FP's is 0.06, i.e. larger than the value 0.05 for the 'optimum' FP, as it should be. This provides a crude estimate of the noise contribution to the width of the FP of about 0.03–0.04, which then implies a similar range of values for the intrinsic width of the FP.

In Table 8 we show the dispersions around the other fits for all relations that we studied in this paper, and with the present dataset. Clearly, the dispersions around the FP are smaller than those around the $L-R$ and $L-\sigma$ relations, for all types of profile fitted. The differences in the dispersions around the $L-R-\sigma$ relations are striking. They show that the King profile not only provides the best description of the central, regular parts of galaxy clusters, but that it also provides a significantly narrower FP than any other of the currently popular profiles.

Table 8. Orthogonal dispersions around the three fitted relations for the MIDWW coefficients. and

	$L-R-\sigma$	$L-R$	$L-\sigma$
King profile	0.05	0.08	0.14
Hubble profile	0.09	0.11	0.14
Virial coeff. & King profile	0.12	0.12	0.17
de Vaucouleurs profile	0.14	0.14	0.14

One might think that the large dispersion in the L - σ_V relation could be partly due to systematic errors in σ_V that are due to contaminating groups of galaxies projected onto the cluster core. Such galaxies could be falling into the cluster and would not be virialized in the cluster potential. However, that is not likely to be an important effect, because the velocity dispersions vary by only a few percent if we exclude the emission-line galaxies, which are the ones suspected to be on fairly radial, infalling orbits (see, e.g., paper III). Apparently our selection of the most regular (i.e. probably virialized) cluster cores, has already minimized this effect. The fact that the scatter around the FP appears to increase when lower-contrast and less regular clusters are included (see Fig. 5) could partly be due to such contaminating galaxies.

On the other hand, the increase of the scatter when lower-contrast and less regular clusters are included could equally well be the result of the fact that these are apparently less well relaxed. The larger dispersion around the FP for the latter clusters is not very likely to be due to relatively larger formal uncertainties in L , R or σ , as inspection of Tab.1 will show.

We conclude that a significant part of the dispersion of clusters around the FP is intrinsic. As we discussed earlier, there are many physical effects that may be responsible for the intrinsic width of the FP: structural differences among clusters, differences in virialization state, and peculiar velocities with respect to a uniform Hubble flow.

Deviations from a pure Hubble flow result in errors in the distance of clusters, δD , which translate into an error $\delta L/L = 2 \delta D/D$ and an error $\delta R/R = \delta D/D$. Therefore the orthogonal intrinsic dispersion around the FP of 0.03–0.04 translates into a dispersion in the L -direction of about 0.05. As our clusters are at an average cz of 20000 km s^{-1} , it is thus unlikely that they have peculiar velocities that greatly exceed 1000 km s^{-1} , as those would induce a larger dispersion around the FP than we observe. This is in agreement with S93 and with the recent estimates based on Tully-Fisher galaxy distances by Bahcall & Oh (1996).

6. Conclusions

We have re-examined the evidence for the existence of a Fundamental Plane (FP) for galaxy clusters, using the new data from the ESO Nearby Abell Cluster Survey (for velocity dispersions and correction for field contamination), and the Cosmos Galaxy Catalogue (for the characteristic radii of the galaxy distributions and the luminosities). We have derived the luminosities, radii and velocity dispersions for our dataset of 29 rich clusters in a homogeneous manner, and we have studied the correlations between these parameters. Our clusters are found to define a quite narrow FP, which confirms the result obtained earlier by S93.

Our result is qualitatively similar to that of S93 although there are quantitative differences that are partly due to the use of different profiles to describe the projected galaxy distribution. On the other hand, our result appears to indicate that the FP for galaxy clusters is significantly different from that for elliptical galaxies. However, more work is needed to establish accurately the qualitative difference between the two, which is a prerequisite for a more detailed understanding of the physical implications of the difference.

The FP that we find for our galaxy clusters differs from the virial prediction, primarily in the sense that the cluster luminosity appears to vary linearly, rather than quadratically, with velocity dispersion. There are several possible effects that could be responsible for that. E.g., cluster cores may have a variety of dynamical structures, or M/L may not be constant, or they may not all be fully virialized, (or combinations of these). Assuming that non-constant M/L is the only reason for the difference between the observed FP and the virial prediction, we estimate that the M/L ratio of rich clusters varies by at most a factor of 2 to 3.

We conclude that a significant part of the observed scatter around the FP is likely to be intrinsic. However, there may also be a contribution from distance errors that are induced by peculiar velocities of clusters with respect to the Hubble flow. Assuming that all the intrinsic scatter in the FP is due to deviations from a pure Hubble flow, we can set an upper limit to the typical cluster peculiar velocities of about 1000 km s^{-1} , in agreement with other, independent results.

Acknowledgements. CA, AM, AB and PK acknowledge financial support from the French GDR Cosmologie and INSU. AM also acknowledges financial support by Leiden Observatory. CA thanks also A. Maucherat, M. Bout and J.M. Deltorn for helpful discussions.

References

- Abell G.O., Corwin H.G., Olowin R.P., 1989, ApJS 70, 1
- Adami C., Mazure A., Katgert P., Biviano A., 1998, A&A submitted: paper VII
- Bahcall N.A., Oh S.P., 1996, ApJ 462, L49
- Beers T.C., Flynn K., Gebhardt K., 1990, AJ 100, 32
- Bender R., Burstein D., Faber S.M., 1993, ApJ 399, 462
- Biviano A., Katgert P., Mazure A. et al. 1996, A&A 321, 84: paper III
- Bonnet H., Mellier Y., Fort B., 1994, ApJ 427, L83
- Bruzual G., Spinrad H., 1978, ApJ 220, 1
- Burstein D., Heiles C., 1982, AJ 1165, 87
- Caon N., Capaccioli M., d'Onofrio M., 1993, MNRAS 265, 1013
- Capelato H.V., de Carvalho R.R., Carlberg R.G., 1995, ApJ 451, 525
- Carlberg R.G., Yee H.K.C., Ellingson E. et al. 1996, ApJ 462, 32
- den Hartog R., Katgert P., 1996, MNRAS 279, 349
- de Vaucouleurs G., 1948, C.R. 227, 586
- Djorgovski S., Davis M., 1987, ApJ 313, 59

- Dressler A., Faber S.M., Burstein D. et al. 1987, ApJ 313, L37
- Ellis R.S., Colless M., Broadhurst T., Heyl J., Galzebrook K., 1996, MNRAS 280, 235
- Faber S., Jackson R., 1976, ApJ 204, 668
- Fadda D., Girardi M., Giuricin G., Mardirossian F., Mezzetti M., 1996, ApJ accepted
- Fletcher R., 1970, Comput.J. 13, 317
- Frei Z., Gunn J., 1994, AJ 108, 1476
- Girardi M., Fadda D., Giuricin G. et al. 1996, ApJ 457, 61
- Gullixson C.A., Boeshaar P.C., Tyson J.A., Seitzer P., 1995, ApJS 99, 281
- Graham A., Lauer T.R., Colless M., Postman M., 1996, ApJ 465, 534
- Guzman R., Lucey J.R., Bower R.G., 1993, MNRAS 265, 731
- Heydon-Dumbleton N.H., Collins C.A., MacGillivray H.T., 1989, MNRAS 238, 379
- Isobe T., Feigelson E.D., Akritas M.G., Babu G.J., 1990, ApJ 364, 104
- Jørgensen I., Franx M., Kjaergaard P., 1996, MNRAS 280, 167
- Katgert P., Mazure A., Perea J. et al. 1996, A&A 310, 8: paper I
- Katgert P., Mazure A., den Hartog R. et al. 1997, A&A in press: paper V
- King I.R., 1962, ApJ 62, 471
- Kormendy J., Djorgovski S., 1989, ARA&A 27, 235
- Lang K.B., 1980, Astrophysical formulae, Springer Verlag, Berlin, Heidelberg, New-York, Second Edition
- Lax D., 1985, J.Am.Stat.Assoc. 80, 736
- Levine S. E., Aguilar L.A., 1996, MNRAS 280, L13
- Lumsden S.L., Collins C.A., Nichol R.C., Eke V.C. Guzzo L., 1997, MNRAS 290, 119
- Mazure A., Katgert P., den Hartog R. et al. 1996, A&A 310, 31: paper II
- Navarro J.F., Frenk C.S., White S.D.M., 1996, ApJ 462, 563
- Nelder J.A., Mead R., 1965, Comput.J. 13, 317
- Pahre M.A., Djorgovski S.G., de Carvalho R.R., 1995, ApJ 453, L17
- Pahre M.A., 1996, BAAS 189, no 29.05
- Renzini A., Ciotti L., 1993, ApJ 416, L49
- Schaeffer R., Maurogordato S., Cappi A., Bernardeau F., 1993, MNRAS 263, L21: S93
- Schechter P., 1976, ApJ 203, 297
- Stein P., 1996, A&A accepted
- Struble M.F., Rood H.J., 1991, ApJS 77, 363
- Tully R.B., Fisher J.R., 1977, A&A 54, 661
- West M.J., Oemler A., Dekel A., 1989, ApJ 346, 539